Reviews in Mineralogy & Geochemistry
Vol. 87 pp. 405-429, 2022

Nucleation, Growth, and Crystallization in Oxide Glass-formers. A Current Perspective

Maziar Montazerian and Edgar Dutra Zanotto*

Center for Research, Technology and Education in Vitreous Materials (*CeRTEV*),
Department of Materials Engineering (*DEMa*)
Federal University of São Carlos (*UFSCar*)
São Carlos, SP, 13.565-905
Brazil

**dedz@ufscar.br*

1. INTRODUCTION

Vitrification from the molten state hinges on averting crystallization during the cooling path. On the other hand, critical natural processes, such as the formation of snow and igneous rocks, like obsidian, and technological operations, for example, solidification of metallic alloys and glass ceramization, illustrate the utmost importance of crystallization in our environment and technology. The structural rearrangements fostered by crystal nucleation and growth cause drastic changes in the macroscopic properties of glass-forming melts and magmas. In this article, we summarize and discuss the applicability of the most accepted models to describe crystal nucleation, growth, and overall crystallization in glass-forming systems. We also focus on the significant progress achieved in the understanding of crystallization over the past few decades through the combined use of theoretical models and experiments. Additionally, we highlight selected open problems and directions for future studies.

When a melt is cooled below its liquidus temperature, it becomes a supercooled liquid (SCL) from which one or more crystalline phases will tend to form. This process takes place in two steps; the formation of crystal clusters (nucleation) and their subsequent evolution to macroscopic crystals (growth). The combination of crystal nucleation and growth leads to the phenomenon called crystallization. Crystallization counteracts vitrification, i.e., the (temporary) freezing of a melt into a glass. Hence, prevention of crystallization upon cooling of any liquid, or upon heating gels, gives rise to a glass. On the other hand, uncontrolled crystallization, devitrification, may occur upon heating a glass (Zanotto and Mauro 2017; Zheng et al. 2019). Eight decades ago, G. W. Morey (1938) stated that "Devitrification is the chief factor which limits the composition range of practical glasses, it is an ever-present danger in all glass manufacturing and working, and takes place promptly with any error in composition or technique." Figure 1 shows a naturally occurring and partially crystallized volcanic glass, called obsidian.

Technological breakthroughs, marked by high-tech industrial processes and devices, require a plethora of novel materials, which include glasses and glass-ceramics with unusual microstructures and enhanced properties, such as high transparency, bioactivity, ionic conductivity, and machinability, sometimes combined with adequate dielectric, magnetic, chemical, mechanical, or thermal shock resistance (Zanotto 2010; Montazerian et al. 2015). To meet this demand, significant efforts have focused on the synthesis of new glasses and

1529-6466/22/0087-0009$05.00 (print)
1943-2666/22/0087-0009$05.00 (online)
http://dx.doi.org/10.2138/rmg.2022.87.09

Figure 1. Partially devitrified obsidian volcanic glass showing (snowflake) cristobalite crystals of ~1cm.

glass-ceramics. In both cases, crystallization control plays such a decisive role that reliable models of crystallization processes are needed. Hence, knowledge about the possible pathways of crystallization allows one to formulate kinetic criteria to answer some questions such as: "Under what conditions can a liquid be supercooled and transform into a glass?" Or equivalently, "under what conditions is crystallization expected to occur on the cooling path?" In attempts to produce new glasses, crystal nucleation and growth must be avoided. Conversely, controlled crystallization can be used to synthesize fully crystallized or semi-crystalline glass-ceramics (Montazerian et al. 2015). Several monographs provide detailed information on these materials (Höland and Beall 2012; Gutzow and Schmelzer 2013; Zanotto 2013; Neuville et al. 2017).

However, these technological aspects represent only one side of the pervasive scientific interest in the kinetics of nucleation and crystallization in glasses. In addition to their practical relevance, the highly viscous glass-forming supercooled liquids serve as remarkable experimental models of metastable systems, in which crystallization processes can be initiated, accelerated or delayed. These processes can thus be studied conveniently under widely different conditions on a laboratory timescale. Such analyses also include the crystallization kinetics versus the thermal history of the sample. For this reason, glass-forming liquids have served as *guinea pigs* for testing crystal nucleation and growth theories, providing a deeper insight into different phase transformation processes. And lastly, controlled crystallization often produces uniquely beautiful (and frequently hidden) nano- and microstructures, as demonstrated by Zanotto (2013), which serves as an additional motivation to pursue research in this endless, albeit highly gratifying quest to unveil the deeply hidden intricacies of glass crystallization and the resulting properties of glass-ceramics.

Preventing or inducing controlled crystal nucleation and growth in a glass (or more correctly in a supercooled liquid, SCL) requires a theoretical understanding of these complex phenomena. Therefore, this article outlines the basic fundamental aspects of the crystallization theory of supercooled oxide glass-forming liquids. Section 2 begins with a description of crystal nucleation kinetics in glass-forming liquids. In Section 3, we provide an overview of the basic modes of crystal growth. Section 4 describes the overall crystallization kinetics, i.e., the evolution of the volume fraction of crystalline phases as a function of time. In this regard, we also dwell on glass-forming ability on the cooling path, and glass stability on heating. In addition to some well-established results, we also discuss open problems and possible approaches to their resolution. In Section 5, a summary of selected results and perspectives for future developments completes this article.

TABLE OF SYMBOLS

ΔG	Gibbs free energy difference	T_m	Melting temperature
R	Ideal gas constant	Δh_m	Heat of melting of one crystal phase particle
A	Nucleus surface area	q_m	Heat of melting
N	Number of particles in the nucleus	N_A	Avogadro's number
$\Delta\mu$	Chemical potential difference	ς	Correction factor that varies in the range 0.4 to 0.6
μ_l	Chemical potential of liquid	f	Fraction of preferred growth sites
μ_{cr}	Chemical potential of crystal	Δs_m	Entropy of melting
σ	Electrical conductivity or surface free energy	C_2 , C_3	Parameters determing the time required for the formation of the two-dimensional nucleus
C_α	Particle number density in the crystal cluster	B	Combination of parameters proportional to the effective diffusion coefficient
P	Pressure	$<R>$	Average size of the nuclei
T	Temperature	N	Number of supercritical nuclei
G	Gibbs free energy	dt'	time-interval
R_c	Critical radius	V	Volume
ΔG_c	Change in the Gibbs free energy	V_n	Volume crystallized
n_i	Number of particles in the cluster	ω_n	Shape factor
W	Work	$\alpha_n(t)=(V_n(t)/V)$	Time-dependent crystallized fraction
W_c	Work of critical cluster formation	N_0	Number of supercritical clusters
τ	Relaxation time	n	Number of independent spatial directions
J	Rate of formation of supercritical clusters	a	Activity
J_s	Steady-state nucleation rate	T_b	Stokes-Einstein breakdown temperature
t	Time	T_g	Glass transition temperature
C_1	Parameter	T_K	Kauzmann temperature
n_c	Number of particles in a cluster of critical size	Φ	Catalytic activity factor of a heterogeneous nucleation core
τ_R	Maxwellian relaxation time	CRR	Cooperatively rearranging regions
η	Newtonian viscosity	TKS	kinetic spinodal temperature
G_S	Shear modulus	T_{gr}	Reduced glass transition temperatures
t_{ind}	Induction time	GFA	Glass-forming ability
dN	Change of number of clusters of critical size	GS	Glass stability
dt	Time interval	D_u	Diffusion coefficients from crystal growth rates
k_B	Boltzmann's constant	D_η	Diffusion coefficients from viscosity
D	Diffusion coefficient	T_d	Decoupling temperature
d_0	Diameter	CCR	Critical cooling rate

2. CRYSTAL NUCLEATION AND CLASSICAL NUCLEATION THEORY

Microscopy techniques are commonly used to determine crystal nucleation rates in supercooled liquids. The simplest and most used method is to perform heat treatments for different periods at a given temperature, then develop the (nanosized) crystal clusters at a higher temperature, and finally quench the specimens to room temperature. This is the so-called development or Tammann method. The treated samples are then polished for microscopic analysis, where the crystal numbers and sizes are measured. The so-called Tammann method (1898) is commonly used to determine the number density of supercritical nuclei. The number of crystals per unit volume is called crystal number density, N, which is measured at different nucleation times to envisage the variation of N versus time, t. The nucleation rate is the slope of the N vs. t plots. A broad range of nucleation can be determined by this method. For example, the maximum crystal nucleation rates for oxide glasses vary between 10^{1} $m^{-3}{\cdot}s^{-1}$ to 10^{17} $m^{-3}{\cdot}s^{-1}$ (Fokin et al. 2006).

The physical nature of nucleation phenomena, in general, and crystal nucleation in supercooled liquids, in particular, was first described by J. W. Gibbs (1926). His basic idea can be illustrated by the free energy change, ΔG, during crystal cluster formation:

$$\Delta G = n\Delta\mu + \sigma A,\ \Delta\mu=\mu_{cr}-\mu_{l},\ A=4\pi R^2,\ n=\frac{4\pi}{3}C_{\alpha}R^3 \quad (1)$$

In formulating Equation (1), it is assumed that spherical crystalline nuclei form in an initially homogeneous liquid. These nuclei are described by their radius, R, surface area, A, and the number, n, of particles (atoms, molecules or the basic structural units of the crystalline phase) they contain. In Equation (1), $\Delta\mu$ (<0) is the difference of the chemical potentials per particle in the liquid (μ_l) and the crystal (μ_{cr}), σ is the interfacial energy, and C_α is the particle number density in the crystal cluster. It is also assumed that the elastic strain energy—due to the density difference between the supercooled liquid and the crystalline solid—immediately decays due to liquid flow and does not interfere with the nucleation process. Within these assumptions, this equation is valid only for the simplest case of crystallization when the liquid and crystal have the same chemical composition. This kind of crystallization is denoted as *polymorphic* or *stoichiometric.* Furthermore, it is assumed that the properties of the crystal clusters are size-independent. Qualitatively, the situation does not change for *incongruent* crystallization when the crystal and liquid phases have different compositions.

According to thermodynamic evolution criteria, at constant pressure, P, and temperature, T, spontaneous macroscopic processes are tied to a decrease in the Gibbs free energy, G, of the system. For this reason, the function $\Delta G = \Delta G(R)$ takes on the shape shown in Figure 2a because the thermodynamic driving force for crystallization, $\Delta\mu$, is negative ($\mu_{cr}<\mu_l$). In this case, cluster formation and growth is accompanied by a decrease in the Gibbs free energy because the surface term in the expression for ΔG is positive. In other words, the tendency for decreasing the Gibbs free energy is counteracted by the surface term, i.e., the surface contribution initially leads to an increase in ΔG with increasing crystal size. Therefore, small crystal clusters formed in the system disappear and only clusters larger than a critical size, R_c, can grow to macroscopic dimensions. As demonstrated in Figure 2a, the critical cluster size is defined by the maximum of $\Delta G(R)$. Systems showing such behavior are denoted as metastable. Metastable states are stable with respect to small fluctuations (generating clusters with sizes $R<R_c$) but unstable with respect to larger fluctuations leading to clusters with sizes $R>R_c$. Thus, viable (supercritical) crystal clusters that are capable of deterministic growth must exceed a certain minimum size. This phenomenon was predicted more than 100 years ago and is now seen directly in molecular dynamics simulations, e.g. Prado et al. (2019). It is this criticality that determines the decisive impact of these embryos (sub-critical) and nuclei (supercritical) on the nucleation processes (Kashchiev 2000; Kelton and Greer 2010; Neuville et al. 2017).

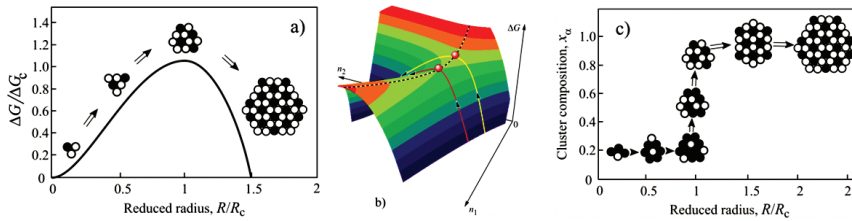

Figure 2. The classical model of nucleation and possible generalizations. **(a)** With only one parameter used to describe the state of the cluster. **(b)** Change of Gibbs free energy in cluster formation when more than one parameter is used. **(c)** An alternative view to the classical scenario of crystallization in multicomponent liquids where both the size and composition change (Schmelzer and Schick 2012).

Taking the chemical potential difference and the interfacial energy as size-independent (i.e., employing the so-called "capillarity" approximation), one can derive the critical cluster size and the value of ΔG_c at the critical size from the extreme condition $\Delta G = 0$. These parameters are thus given by:

$$R_c = \frac{2\sigma}{c_\alpha \Delta\mu} \quad \Delta G_c = \frac{1}{3}\sigma A_c = \frac{16\pi}{3}\frac{\sigma^3}{\left(c_\alpha \Delta\mu\right)^2} \quad A_c = 4\pi R_c^2 \tag{2}$$

The concepts discussed above are illustrated in Figure 2a within the framework of the classical model of nucleation, whereby the change in the Gibbs free energy of cluster formation reaches a maximum $\Delta G = \Delta G_c$ for the critical cluster size, $R = R_c$. In this model, clusters grow or decay while preserving their properties, so that size is the only parameter specifying their state (Schmelzer and Schick 2012).

A more realistic picture of cluster formation is presented in Figure 2b, where not only the size but also the composition (described by the number of particles, n_i, of two components) of the cluster may change. In this case, the critical cluster corresponds to a saddle point of the Gibbs free energy surface. The evolution to the new phase via the saddle is shown by the red curve. Figure 2c shows an alternative to the classical picture, which is similar to the spinodal decomposition (cf. Gutzow and Schmelzer 2013). In this case, the composition of the crystal cluster changes when a nearly constant size is reached and only after completion of this process are the kinetics governed by the growth of clusters with a roughly constant composition. In several cases in multicomponent systems (Gutzow and Schmelzer 2013), the latter path of evolution (Fig. 2c)—and not the classical picture (Fig. 2a)—may dominate phase transformation.

Critical clusters form by stochastic thermal fluctuations. According to underlying assumptions of statistical physics, the probability of such fluctuations can be expressed as a function of the minimum work of a reversible thermodynamic process. The minimum work to form a critical cluster is $W_c = \Delta G_c$, where ΔG_c is given by Equation (2). This quantity, W_c, the work of critical cluster formation, plays a decisive role in nucleation theory. Then, after a certain time interval, τ (nucleation time-lag), the rate of nucleation, J (the number of supercritical clusters formed per unit time in a unit volume of the liquid), approaches a constant value, the steady-state nucleation rate, J_s. In an early description of this initial period of nucleation by Zeldovich (cf. Gutzow and Schmelzer 2013), the nucleation rate as a function of time, t, was expressed by the simplified relation

$$J(t) = J_S \exp\left(-\frac{\tau}{t}\right) \tag{3}$$

where τ is the (true) nucleation time-lag.

The initial stage of nucleation observed in experiments is often described by the Kashchiev relation (Kaschiev 2000),

$$N(t) = J_s \tau \left[\frac{t - t_0}{\tau} - \frac{\pi^2}{6} - 2\sum_{m=1}^{\infty} \frac{(-1)^m}{m^2} \exp\left(-m^2 \frac{t - t_0}{\tau} \right) \right], t > t_0 \text{ and } N = 0, t \le t_0 \quad (4)$$

where t_0 is the so-called time shift, the observed shift between the N versus time curves experimentally obtained by the double-stage or development method and after single-stage treatments (when a powerful electron microscope is available). This mathematical equation gives a relation for the number, $N(t)$, of supercritical crystallites dependent on time, t. For longer times than the experimental induction time (t_{ind}) sometimes observed in $N(t)$ versus time plots, Equation (4) can be approximated by

$$N(t) \cong J_s (t - t_{ind-dev}) \quad t_{ind-dev} = \frac{\pi^2}{6}\tau + t_0 \quad (5)$$

We emphasize that there is a difference between the $t_{ind\text{-}dev}$ (observed after nucleation + development treatments) from the real nucleation induction time, $t_{ind\text{-}nucleation}$ that would be obtained from a single-stage treatment. This is exactly what Equations (4) and (5) assume and is illustrated schematically in Figure 3. In this figure, t_1 is the time when the first critical nucleus is formed.

Over a sufficiently long time**,** Equations (3–5) approach steady-state nucleation conditions, i.e., $(dN/dt) = J_s = \text{constant}$. With $W_c = \Delta G_c$, the steady-state nucleation rate, J_s, can be written as (Gutzow and Schmelzer 2013)

$$J_s = J_0 \exp\left(-\frac{\Delta G_c}{k_B T} \right) = J_0 \exp\left(-\frac{W_c}{k_B T} \right) = J_0 \sqrt{\frac{\sigma}{k_B T}} \left(\frac{D}{d_0^4} \right) \quad (6)$$

where D is the effective diffusion coefficient controlling nucleation and d_0 is a size parameter or atomic jump distance. Experimental results that illustrate the establishment of a steady-state nucleation rate and its dependence on temperature are shown in Figure 4.

For the case shown in Figure 2a (congruent crystallization, assuming that the cluster properties do not change with size and are the same as those of the new macroscopic phase), D in Equation (6) is the diffusion coefficient of the structural building units in the liquid, and d_0 is their diameter. If several components of the liquid diffuse independently, D must be replaced by an effective diffusion coefficient, which is a combination of the partial diffusion coefficients and the concentrations of the different components in the liquid, and d_0 must be replaced by the average size of these independently moving species (Gutzow and Schmelzer 2013).

In applications of this theory, due to the scarcity of diffusion data for oxide glass-formers, it is often *assumed* that the diffusion coefficient can be replaced by the Newtonian shear viscosity, η, via the Stokes–Einstein–Eyring equation:

$$D \cong \frac{k_B T}{d_0 \eta} \quad (7)$$

However, its applicability for temperatures around the glass-transition temperature (where homogeneous crystal nucleation is commonly observable) has been questioned even for stoichiometric systems, where decoupling of structural relaxation (expressed by viscosity) and atomic transport (represented by the diffusion coefficient) has often been reported in crystal growth experiments (e.g., Nascimento et al. 2011). However, to the best of our knowledge, **such decoupling has not yet been proved for nucleation processes,** and this is thus a relevant open problem.

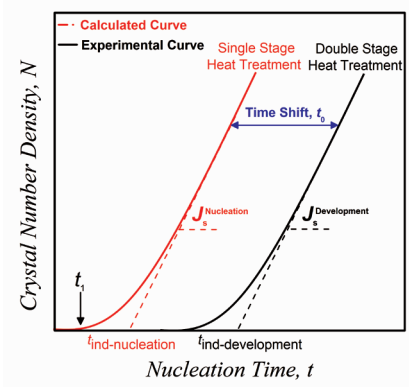

Figure 3. Schematic illustration showing the variation of crystal number density vs. nucleation time. Here, the difference between nucleation induction time in two conditions, viz. double stage heat treatment—laboratory nucleation experimentation—and single-stage heat treatment, which is normally obtained by calculations $J_s^{\text{development}} = J_s^{\text{Nucleation}}$

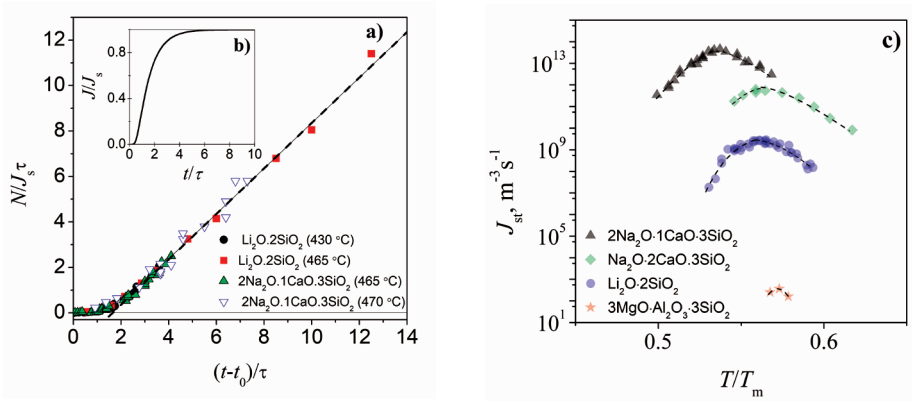

Figure 4. Experimental nucleation rate data for several silicate glasses. **(a)** Reduced crystal number density, $(N(t)/J_s\tau)$, versus reduced nucleation time, $((t-t_0)/\tau)$. The **solid line** is the master curve calculated from Equation (4). **(b)** Reduced nucleation rate versus reduced nucleation time calculated from Equation (4). **(c)** Experimental steady-state nucleation rate, J_s, versus reduced temperature, T/T_m, for four stoichiometric glasses. T_m is the melting temperature. [Reprinted from Fokin VM et al. (2006) Homogeneous crystal nucleation in silicate glasses: A 40 years perspective. J Non-Cryst Solids 352:2681–2714. Copyright (2006), with permission from Elsevier.]

The application of this expression is even more questionable for multicomponent systems. i.e., non-stoichiometric systems in which more than one phase crystallize upon heating (Fokin et al. 2019; Macena et al. 2020). Another issue is related to the case of highly viscous glass-forming melts, for which a non-Newtonian viscosity should be employed to describe viscous flow (Gutzow and Schmelzer 2013). Leaving aside the above-listed reservations, by using the Stokes–Einstein–Eyring relationship, the following expression results for the steady-state nucleation rate:

$$J_s = \frac{\sqrt{\sigma k_B T}}{d_0^5 \eta} \exp\left(-\frac{\Delta G_c}{k_B T}\right) \tag{8}$$

To apply Equation (8) to the interpretation of experimental data, one has to determine the work of critical cluster formation, $W_c = \Delta G_c$, i.e., to specify the thermodynamic driving force, $\Delta\mu$, and the interfacial energy, σ in Equation (2). Assuming that the properties of the crystalline clusters are the same as those of the isochemical macroscopic crystals, one arrives at the simplest approximation by a Taylor expansion of $\Delta\mu(T)$ in the vicinity of the melting temperature:

$$\Delta\mu(T)=\Delta h_{\mathrm{m}}\left(1-\frac{T}{T_{\mathrm{m}}}\right) \tag{9}$$

where Δh_{m} is the enthalpy of melting per structural unit of the crystal and T_{m} is the melting temperature. This expression gives an upper bound for $\Delta\mu(T)$ because it neglects the difference in the specific heats of the crystal and SCL.

Since the interfacial energy of the critical nucleus is not directly measurable, it is normally evaluated using the Stefan–Skapski–Turnbull rule (Gutzow and Schmelzer 2013)

$$\sigma=\varsigma\frac{q_{\mathrm{m}}}{\mathrm{N_A^{1/3}}\nu_{\mathrm{m}}^{2/3}},\ q_{\mathrm{m}}=\mathrm{N_A}\Delta h_{\mathrm{m}} \tag{10}$$

In Equation (10), q_{m} is the molar enthalpy of melting, $\mathrm{N_A}$ is Avogadro's number, ν_{m} is the molar volume, and ς is a numerical factor equal to 0.4 to 0.6. By substituting these relations into Equation (8), its temperature dependence can be interpreted. The steady-state nucleation rate J_s is zero at $T=T_{\mathrm{m}}$, where $\Delta\mu=0$, cf. Equation (9). Starting from the melting point, the nucleation rate increases with decreasing temperature because of the decrease in the work of critical cluster formation, given by Equation (2), until this trend is overcompensated by the exponential decrease of the diffusivity (increase of viscosity) and results in a maximum. For typical cases of homogeneous nucleation in oxide glasses, the maximum occurs at $T_{\mathbf{max}}\sim T_{\mathbf{g}}$, which corresponds to supercoolings of 0.5–0.6 T_{m}. (Fokin et al. 2006).

Homogeneous nucleation in supercooled glass-forming liquids. In most cases, using viscosity as a proxy to $D(T)$ and a constant, fitted value of σ, this classical approach gives a good temperature dependence, at least for the high-temperature side above T_{max}, but underestimates the steady-state nucleation rates by **20–55** orders of magnitude, e.g. Fokin et al. (2006). These huge deviations between experiment and theory can be resolved by the introduction of a size or temperature dependence of the interfacial energy, as discussed by Gibbs (1926) and later by others, particularly by Tolman, e.g. Gutzow and Schmelzer (2013). However, this solution does not solve other problems (Fokin et al. 2006), such as the alleged breakdown of the classical nucleation theory (CNT) for temperatures below T_{max} (Cassar et al. 2020). Another possible solution, resulting from computer simulations and density functional computations, consists of accounting for the size dependence, not only of the surface tension, but also of the other properties of the critical clusters. The internal properties of the clusters generally depend on their sizes. Hence, the surface properties, including the surface tension, must also be size-dependent. Thus, this approach also leads to a size dependence of the surface energy.

On the other hand, recent computer simulations favor the validity of CNT. Rather than using approximations or calculated values for the thermodynamic parameters and diffusivities, the CerTEV, São Carlos group employed parameters directly obtained from molecular dynamic simulations, without any fitting parameter, for different substances and demonstrated that the CNT is indeed a powerful predictor of crystal nucleation rates in some reluctant glass-formers, such as L-J, Ge (Tipeev et al. 2018, 2020) and ZnSe (Separdar et al. 2021). These findings should still be tested with regular glass-formers to generalize CNT´s applicability.

With a thermodynamic (generalized Gibbs) approach, which treats the cluster properties as a function of size and degree of supercooling, one concludes that the classical theory—assuming that the clusters have macroscopic properties and employing the capillarity approximation for the interfacial energy—overestimates the work of critical cluster formation, and hence, underestimates the steady-state nucleation rates. Therefore, the classical theory with the capillarity approximation serves as a tool for roughly estimating temperature dependence of nucleation rates, but it must be significantly improved to account for the above-specified effects for a detailed and quantitatively accurate description of the phenomenon (Gutzow and Schmelzer 2013).

Heterogeneous Nucleation. So far, we have considered the case of crystal nuclei that form evenly within a defect-free homogeneous liquid. This mechanism is known as *homogeneous* nucleation. However, nucleation can be readily catalyzed by solid impurities, such as particles embedded in the volume or present on the external surface of glasses. Nucleation originating at such preferential sites is denoted as *heterogeneous* and can be described by the theoretical concepts outlined above if the work of critical cluster formation for homogeneous nucleation, W_c, is replaced by $W_c\Phi$. Here, $\Phi \leq 1$ is the nucleating activity of the heterogeneous nucleation core, and its value depends on the mechanism of catalysis. Heterogeneous nucleation dominates at small supercooling because of the lower work of critical cluster formation than that of homogeneous nucleation. At deep supercoolings, homogeneous nucleation may dominate due to much lower work of critical nucleus formation and the much larger number of sites (all "structural units" of the system) where homogeneous nucleation may proceed (Fokin et al. 2006).

One should note that, in certain cases, the evolution of the crystal phase may not proceed via the red saddle shown in Figure 2b, but via a ridge trajectory indicated by a yellow curve in Figure 2b, if such a trajectory is kinetically favored. This type of behavior may be expected to occur in crystallization occurring at deep supercoolings because of the defective and non-stoichiometric nature of the crystals that might precipitate in the early stages of crystallization (Fokin et al. 2003).

Frequently, several different metastable phases may be formed in the supercooled liquid. As Ostwald suggested many years ago, in such cases the most favorable stable phase is not formed immediately. Instead, the final stable phase frequently crystallizes through several stages in which different metastable phases are formed; this is the so-called Ostwald's rule of stages or Ostwald's step rule.

2.1. Recent findings that warrant further research: Examples of experimental tests

The alleged CNT breakdown at T_{max}. For a variety of oxide glass-forming liquids, the thermodynamic barrier for homogeneous crystal nucleation, W_c, apparently exhibits an unusual increase with decreasing temperatures below the experimental maximum nucleation rate, T_{max} (Fig. 5), ($T_{max} \sim T_g$) which is not compatible with predictions using the CNT. Abyzov et al. (2016) sought possible explanations for the increasing W_c by analyzing whether it could be caused by internal elastic stresses that arise due to density misfits between the crystal and liquid phases. Please recall that this factor was neglected in the derivation of Equation (6).

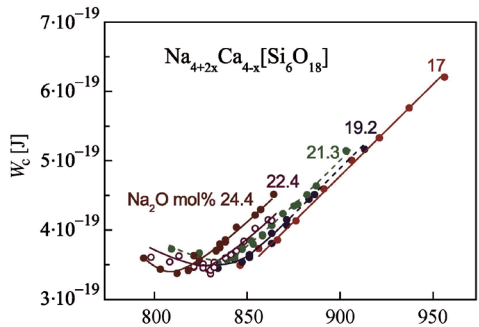

Figure 5. Calculated thermodynamic barrier for nucleation versus temperature for a series of sodium-calcium silicate glasses. W_c exhibits an unusual increase with decreasing temperatures below the maximum nucleation rate, T_{max}. [Reprinted from Abyzov AS et al. (2016) The effect of elastic stresses on the thermodynamic barrier for crystal nucleation. J Non-Cryst Solids 432:325–333. Copyright (2016), with permission from Elsevier.]

For this purpose, the crystal nucleation rate and induction time data for two glasses that display significantly different density misfits between the crystalline and liquid states, lithium and barium disilicates, were employed to determine the work of critical cluster formation, W_c. Quantitative estimates of the effect of the elastic strain energy on W_c were carried out for both glasses. The interplay between stress development and structural relaxation of the SCL was accounted for. Their computations were performed taking into account not only the possibility of precipitation of the most stable crystal phase, but also the fact that different metastable phases might form during the early stages of nucleation. They showed that elastic strain energy indeed reduces the thermodynamic driving force for crystallization, and thus increases the barrier to nucleation. To better illustrate the effect of elastic stress, Figure 6 shows the experimental nucleation rates and the nucleation rates calculated disregarding and accounting for the stresses, and their relaxation for the stable and metastable phases with different melting temperatures, T_m, shown close to the respective curves. In all these cases, the calculated maxima of the nucleation rate are located at temperatures that are lower than the experimental maximum. It is clear that accounting for the elastic strain energy component in the reduction of the thermodynamic driving force decreases the nucleation rates (compare dotted and solid lines). However, as shown by the solid lines and data points, the calculated nucleation rates do not reach the experimental values, and only approach them for lithium disilicate glass (L2S) if a metastable phase having a very low melting point, say 1107 K, appears. Nevertheless, it is important to underline that at 1107 K with any further decrease in temperature, this (invented) metastable phase would be poorly ordered and unstable. Therefore, it seems that the sole effect of elastic strain cannot explain the aforementioned unusual behavior of the thermodynamic barrier at T_{max}. **Hence, a comprehensive explanation for this phenomenon is still lacking** (Abyzov et al. 2016).

In another attempt to explain the break at T_{max}, Fokin et al. (2016) emphasized that the CNT fails to describe crystal nucleation rates in supercooled liquids if one uses a fixed size, d_o, of the "structural units." Some results for silicate glasses support the view that, even for the so-called

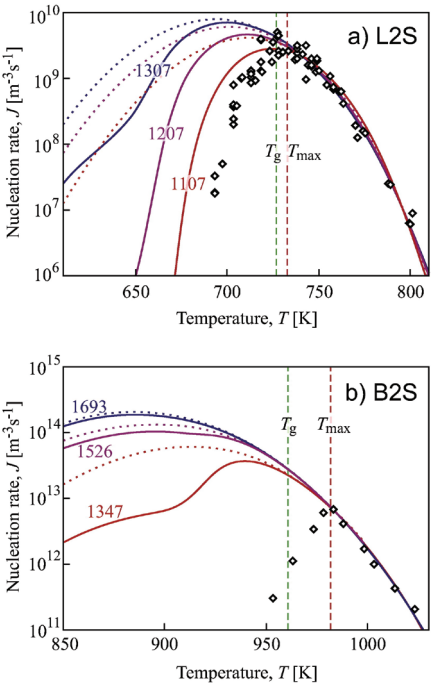

Figure 6. Nucleation rates for lithium disilicate (LS2) **(a)** and barium disilicate (B2S) **(b)** versus temperature. The symbols show measured values, the **dotted lines** show nucleation rates calculated without accounting for stresses. The **solid lines** show the rates taking into account the elastic stresses and their relaxation for the stable macroscopic phase (T_m = 1307 °C for LS2 and T_m = 1693 °C for B2S) and two metastable phases having different melting temperatures, T_m. [Reprinted from Abyzov AS et al. (2016) The effect of elastic stresses on the thermodynamic barrier for crystal nucleation. J Non-Cryst Solids 432:325–333. Copyright (2016), with permission from Elsevier.]

case of stoichiometric (polymorphic) crystallization, the nucleating phase may have a different composition and/or structure as compared to the parent glass and the evolving macroscopic crystalline phase. This finding perhaps explains the discrepancies between calculated (by CNT) and experimentally observed nucleation rates in deeply undercooled glass-forming liquids (Fokin et al. 2007). Therefore, to reconcile the experimental data and CNT, Fokin et al. (2016) assumed an abnormal increase in the size of the structural units that control nucleation with decreasing temperature for temperatures below T_{max}. This hypothesis was tested for several glass-forming liquids, where crystal formation proceeds by bulk homogeneous nucleation. This study could perhaps explain the temperature dependence of the nucleation rate in the range of $T < T_{max}$, where the description of the nucleation rate by CNT drastically fails. The size of the structural units could be related to the size of the cooperatively rearranging regions (CRR), which are linked to dynamic heterogeneities in glass-forming liquids.

Over the past few decades, a very important discovery in the study of glass-forming liquids was the finding of dynamic heterogeneity referring to the spatiotemporal fluctuations in local dynamics (Ediger 2000). The growth of the dynamic correlation length of the CRR as the temperature decreases toward the glass transition provides a possible approach to understand the dramatic slowdown of dynamics during vitrification (Flenner and Szamel 2010). Thus, more attention has been given to investigating the correlation between structural relaxation with dynamic heterogeneity and crystal nucleation in glass-forming liquids (e.g., Berthier 2011; Henritzi et al. 2015; Gupta et al. 2016). For example, Gupta et al. (2016) referred to the temperature at which the classical critical nucleus size is equal to the average size of the CRR in a supercooled liquid as a "cross-over" temperature. They showed, for the first time, using published nucleation rate, viscosity, and thermo-physical data that the cross-over temperature for the lithium disilicate melt is very close to the temperature corresponding to the maximum in the experimentally observed nucleation rates. They suggested that the abnormal decrease in nucleation rates below the cross-over temperature is most likely because, in this regime, the CRR size controls the critical nucleus size and the nucleation rate. This finding links, for the first time, measured nucleation kinetics to the dynamic heterogeneities in a supercooled liquid (Gupta et al. 2016).

A more straightforward explanation was proposed recently by Cassar et al. (2020). They analyzed literature data for 6 glasses using a rigorous protocol and indicated that the alleged breakdown at T_{max} is apparent only because most researchers are not patient to give long enough heat treatments to reach the steady-state regime. In other words, in most cases, incorrect nucleation rate data have been used to analyze the dynamics below T_{max}. **This problem warrants further investigation.**

I_{max} versus T_{gr}. Recently, Abyzov et al. (2018) employed the Classical Nucleation Theory using a characteristic value of the pre-exponential constant and an average (temperature-dependent) interfacial energy and derived an expression to estimate the maximum nucleation rates, I_{max}, as a function of the reduced glass transition temperatures, $T_{gr} \equiv T_g/T_m$ (T_g is the laboratory glass transition temperature and T_m is the melting point or *liquidus* temperature). The theoretical predictions were surprisingly good for 51 out of 54 silicate glass-formers tested and describe the experimental trend well that I_{max} strongly decreases with increasing T_{gr} (Fig. 7*)*. This trend also explains the well-known fact that only silicate glasses having a relatively low T_{gr}**,** $T_{gr} < 0.6$, show internal homogeneous nucleation in laboratory time/sample-size scales (Abyzov et al. 2018).

Nucleation and the Kauzmann paradox. Zanotto and Cassar (2018) have tried to answer the key question whether any liquid can be cooled down below its melting point to the isentropic (Kauzmann) temperature, T_K, without vitrifying or crystallizing. This long-standing problem concerning the ultimate fate of supercooled liquids is one of the fundamental glitches in materials science. They used thermodynamic and kinetic data and well established theoretical models to estimate the T_{KS} (kinetic spinodal temperature, at which the average

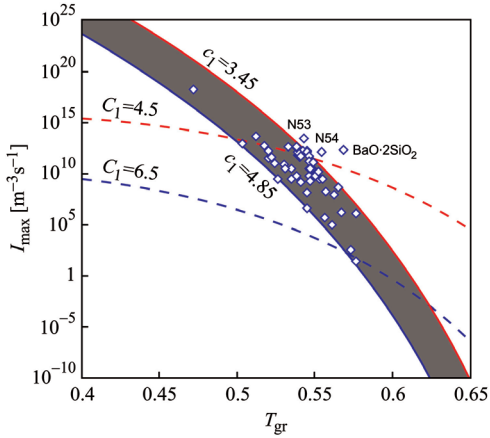

Figure 7. Maximum steady-state nucleation rate, I_{max}, versus reduced glass transition temperature, T_{gr}. The symbols refer to experimental data of 54 silicate glasses. The dashed lines were calculated using **constant** values of $C_1 = c_1\kappa(T_{gr} - 0.556) = 4.5$ (**top dashed red line**) and $C_1 = 6.5$ (**bottom dashed blue line**). The **solid lines** were recalculated for temperature dependent C_1 using $T_{max}(T_{gr}) \approx 10^{24} \exp\left\{-\frac{c_1 + \kappa(T_{gr} - 0.556)}{T_{gr}(1 - T_{gr})}\right\}$, where c_1 and κ are the parameters that best fit the current experimental data, e.g. for $c_1 = 3.45$ (**top solid red line**) and $c_1 = 4.85$ (**bottom solid blue line**). The experimental errors in I_{max} and T_{gr} are of the order of the symbol size. [Reprinted from Abyzov AS et al. (2018) Predicting homogeneous nucleation rates in silicate glass-formers. J Non-Cryst Solids 500:231–234. Copyright (2018), with permission from Elsevier.]

time for the first critical crystalline nucleus to appear becomes equal to the average relaxation time of a supercooled liquid) and the Kauzmann temperature for two substances—a borate and a silicate glass—which show measurable homogeneous crystal nucleation in laboratory time scales, as proxies of these families of glass-formers. For both materials, they found that the T_{KS} are significantly higher than the predicted T_K. Therefore, at ambient pressure, at deep supercoolings before approaching T_K, crystallization wins the race over structural relaxation. Hence, the temperature of entropy catastrophe predicted by Kauzmann cannot be reached for the studied substances; it is averted by incipient crystal nucleation (Zanotto and Cassar 2018). As several approximations were made for the calculations and they required extrapolations to very low temperature, this is still considered an **open relevant problem that warrants further research**. Computer simulations could be particularly relevant to shed light into this problem.

3. BASIC MODELS OF CRYSTAL GROWTH IN SUPERCOOLED LIQUIDS

Microscopy techniques are commonly used to determine crystal growth, $U(T)$, rates in supercooled liquids. The simplest and most used method is to perform heat treatments for different periods at a given temperature and quench the material to room temperature. Samples are then polished for microscopic analysis, where the crystal sizes on the sample surface or in their interior are measured. Then, the growth rates are calculated from the slopes of the crystal size radius versus time plots at different temperatures (Fig. 8). Hot stage microscopes can also be employed, in which case the growing crystals on the sample surface are directly observed *in situ.* Jiusti et al. (2020) have recently shown (Fig. 9) experimental values of crystal growth rates for 20 stoichiometric oxide glass formers. They observed that the temperature of maximum growth rate (T_{max}) lies within the range of 0.90 to $0.98T_L$ for all the materials investigated, whereas the maximum crystal growth rate, $U(T_{max})$, varies seven orders of magnitude. For the sake of simplicity, they used the average value, $T_{max} = 0.94T_L$ in their study for the derivation of their GFA predictor (see Section 4).

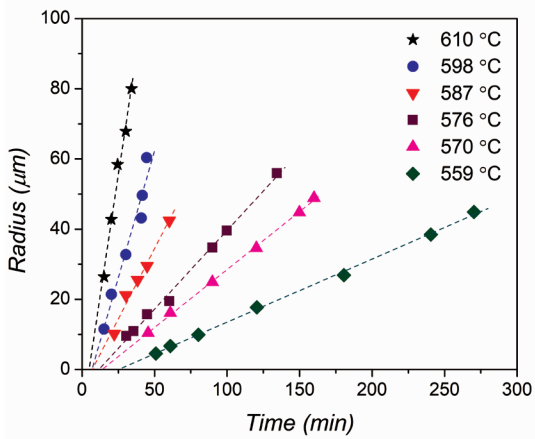

Figure 8. Increase in the crystal radius with time for lithium disilicate glass heat treated at different growth temperatures. [Reprinted from Deubener J et al. (1993) Induction time analysis of nucleation and crystal growth in di- and metasilicate glasses. J Non-Cryst Solids 500:231–234. Copyright (1993), with permission from Elsevier.]

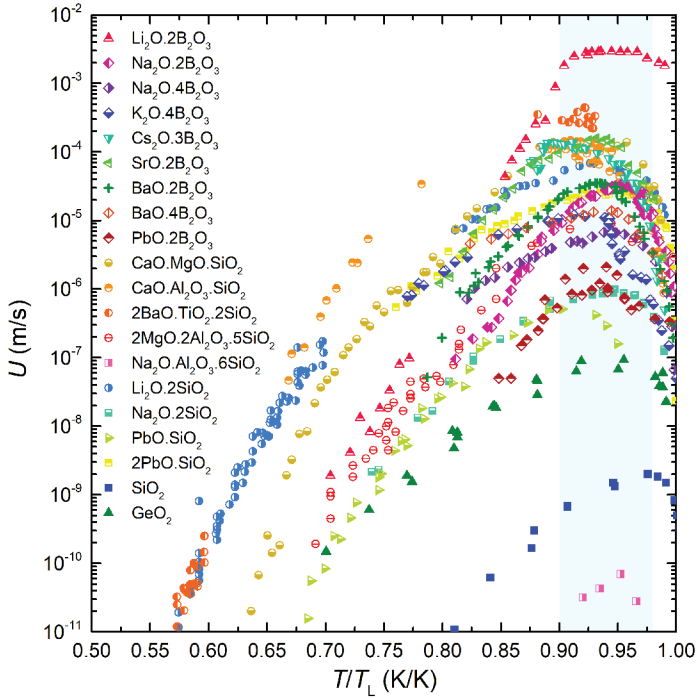

Figure 9. Crystal growth rate versus reduced temperature for 20 stoichiometric oxide glass formers. $U(T_{max})$ always occurs at a temperature between $0.90-0.98T_L$ (**highlighted region**) (Jiusti et al. 2020).

Recently, Reis et al. (2016) proposed and tested a simpler and yet accurate technique capable of determining the crystal growth rate over a fairly wide temperature range by means of a single differential scanning calorimetry (DSC) run. Their method was based on using 50–200 μm thick samples with parallel rough surfaces so that crystal growth is effectively unidirectional and the crystallization fronts have a constant area during the entire crystallization process.

Growth rates are calculated from the expression $U(T) = L \times q \times \mathrm{DSC}(T)/A_{peak}$, where $\mathrm{DSC}(T)$ is the value of the DSC crystallization curve at each temperature T, A_{peak} is the overall peak area, L is half the sample thickness, and q is the heating rate. This method was tested for different values of L and q for three glasses undergoing predominantly surface nucleation, which have distinctly different crystallization behaviors: stoichiometric lithium disilicate and diopside ($CaO{\cdot}MgO{\cdot}2SiO_2$) and a nonstoichiometric lithium-calcium metasilicate. Growth rates spanning temperature intervals of more than 100 K, including temperature ranges where literature data were scarce due to experimental difficulties, were determined using a single DSC run. The resulting $U(T)$ data were compared with literature data obtained using optical microscopy. The growth rates determined using the proposed method showed excellent agreement with the published data for both stoichiometric glasses and only small errors for the nonstoichiometric glass (Reis et al. 2016; Zheng et al. 2019). Hence, one can use one of these techniques to obtain crystal growth rate curves.

It is known that the properties of the crystal-liquid interface have a decisive influence on the kinetics of crystallization. Theoretical treatments of crystal growth have therefore focused closely on the interfacial structure and its effect on crystallization. With the assumption of congruent polymorphic crystallization, three standard models have been developed for treating crystal growth theoretically (e.g., Uhlmann 1982; Jackson 2004). These models are described briefly below:

(i) *Normal growth.* The interface is pictured as rough at an atomic scale. Growth takes place at step sites, which represent a sizable fraction (0.5–1.0) of the interface. Assuming that this fraction does not change appreciably with temperature, the growth rate, $u(T)$, can be expressed as

$$u = f\frac{D}{4d_0}\left[1-\exp\left(-\frac{\Delta\mu}{k_B T}\right)\right] \tag{11}$$

where f, fraction of preferred growth sites, is close to unity and $\Delta\mu$ is treated as a positive quantity.

(ii) *Screw dislocation growth.* This model assumes the interface is smooth but imperfect at an atomic scale. Growth takes place at a few step sites provided by screw dislocations that intersect the interface. The growth rate is still given by Equation (11), where f is now the fraction of preferred growth sites (on the dislocation ledges) at the interface. In this case, f is given approximately by $f \approx (T_m - T)/2\pi T_m$ (Nascimento et al. 2011). More generally, according to Jackson (2004), $f = (\Delta s_m/k_B)\xi$ holds, where Δs_m is the entropy of fusion per particle, and ξ is the number of nearest-neighbor sites in a layer parallel to the surface divided by the total number of nearest-neighbor sites. Factor is the largest for the most closely-packed planes of the crystal, for which it is approximately equal to 0.5.

For $f < 2$, the minimum free energy configuration corresponds to half the available sites being filled and represents an atomically rough surface. In contrast, for $f > 2$, the lowest free energy configuration corresponds to a surface where few sites are filled, and a few units are missing from the completed layer, and which represents an atomically smooth interface. Hence, for materials with $\Delta s_m < 2k_B$, the most closely packed interface planes should be rough. For materials with $\Delta s_m < 4k_B$, the most closely-packed surfaces should be smooth, the less tightly packed surfaces rough, and the growth anisotropy rate large.

(iii) *Surface nucleation or two-dimensional growth.* According to this model, the interface is smooth and perfect at an atomic scale, and thus free of intersecting screw dislocations and growth sites. Growth then takes place by the formation and growth of new two-dimensional nuclei at the interface. In this case, the growth rate is expressed by

$$u = C_3 \frac{D}{4d_0^2} \exp\left(-\frac{C_2}{T\Delta T}\right), \tag{12}$$

where C_2 and C_3 are parameters that determine the time required for the formation of the two-dimensional nucleus relative to that required for its propagation across the interface, respectively.

Possible growth modes are illustrated in Figure 10. Similarly to nucleation, the interplay between increasing driving force for crystallization, $\Delta\mu$, and decreasing diffusion coefficient (or increase in viscosity) with decreasing temperature results in a maximum of the crystal growth rates. This maximum is located at higher temperatures than that of the maximum of the steady-state nucleation rate shown in Figure 4c.

Other growth modes exist which are limited not by processes at the liquid-crystal interface but by atomic transport towards the interface. A specific example is a diffusion-limited segregation, which is of particular importance in multicomponent systems. Accounting for size effects on the growth kinetics, the rate for such a growth mode can be expressed as (e.g., Slezov 1999; Jackson 2004).

$$\frac{dR}{dt} = \frac{B}{R}\left(\frac{1}{R_c} - \frac{1}{R}\right) \tag{13}$$

where B is a combination of parameters describing the liquid under consideration**,** which are proportional to the effective diffusion coefficient governing the rate of supply of the different components to the growing or dissolving cluster.

Equation (13) and its modifications for other growth modes serve as a basis for the theoretical description of the competitive growth of clusters denoted as coarsening or Ostwald ripening. In these late stages of phase formation, larger clusters may continue to grow only when subcritical crystals are dissolved. The theoretical description of this process was first developed by Lifshitz and Slezov (cf. Jackson 2004). Today it is often referred to as the

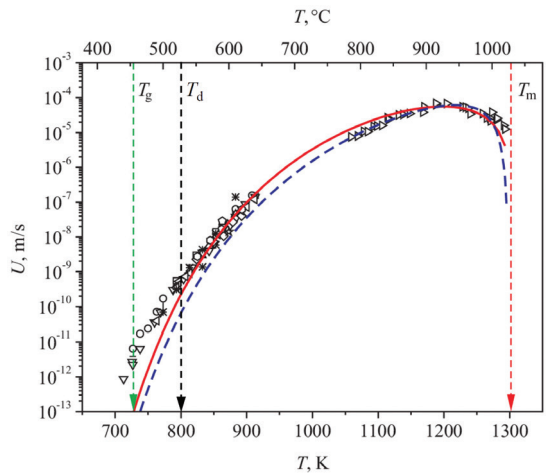

Figure 10. Crystal growth rates for $Li_2O{\cdot}2SiO_2$ glasses obtained by different authors. The lines correspond to the screw dislocation mechanism (**full curve**) and two-dimensional surface nucleated growth (**dashed curve**). (T_d: decoupling temperature, T_g: glass transition temperature, T_m: melting temperature). [Reprinted from Nascimento et al. (2011) Dynamic processes in a silicate liquid from above to below the glass transition. J Chem Phys 135:194703, with the permission of AIP Publishing.]

L(ifshitz)S(lezov)W(agner) theory. This theory provides expressions for the average size, R, and the number, N, of supercritical clusters in the system as a function of time. For diffusion-limited growth (Eqn. 13), one obtains

$$R^3 \propto t, N \propto \frac{1}{t} \tag{14}$$

An account of the effect of elastic stresses on coarsening, which leads to qualitative modifications of the coarsening behavior, is reviewed in (Slezov 1999).

3.1 Experimental tests

Nascimento and Zanotto (2006) have analyzed extensive literature data on crystal growth rate and viscosity in the temperature range between $1.1T_g$ (glass transition temperature) and the melting point of silica (SiO_2). They selected U(T) and η(T) data for the same silica glass type, having similar impurity contents, and confirmed that the *normal growth* model describes the experimental U(T) data quite well in this wide undercooling range. They then calculated effective diffusion coefficients from crystal growth rate, D_U, and from viscosity, D_η (through the Stokes–Einstein/Eyring equation) and compared these two independent diffusivities with directly measured self-diffusion coefficients of silicon and oxygen in the same silica glass type. Their results showed that silicon (not oxygen) controls the diffusion dynamics involved in both crystal growth and viscous flow in undercooled silica. This study not only unveiled the transport mechanism in this important glass-forming material but also validated the use of (easily measured) viscosity to account for the unknown transport term of the crystal growth expression in a wide range of undercoolings (Nascimento and Zanotto 2006).

Later on, Nascimento and Zanotto (2010) analyzed the kinetic coefficient of crystal growth, $U_{kin} \sim \eta^{-\omega}$, proposed by Ediger (2008), which indicated that the Stokes–Einstein/Eyring (SE/E) equation does not describe the diffusion process controlling crystal growth rates in *fragile* glass-forming liquids. U_{kin} was defined by Ediger (2008), using the *normal* growth model and tested for crystal data for inorganic and organic liquids covering a viscosity range of about 10^4–10^{12} Pa.s. Afterwards, Nascimento and Zanotto 2010 revisited their finding considering two other models: the *screw dislocation* (*SD*) and the *two-dimensional surface nucleated* (2D) growth models for nine undercooled oxide liquids, in a wider temperature range, from slightly below the melting point down to the glass transition region T_g, thus covering a wider viscosity range: 10^1–10^{13} Pa.s. Then, they normalized the kinetic coefficient (D_U, which scales with $\eta^{-\omega}$, and the exponent ω supposedly depends systematically on the fragility of the liquid: the greater the fragility, the lower the value of ω) for the SD and 2D growth models. These recalculated kinetic coefficients restored the ability of viscosity to describe the transport part of crystal growth rates ($D_U \sim 1/\eta$, $\omega \sim 1$) from low to moderate viscosities ($\eta < 10^6$ Pa s), and thus demonstrated that the SE/E equation indeed worked well in this viscosity range for all systems tested. For strong glasses, the SE/E equation described low to high viscosities, from the melting point down to T_g. However, for at least three fragile liquids, diopside (for $T_d = 1.08T_g$, $\eta = 1.6 \times 10^8$ Pa s), lead metasilicate (at $1.14T_g$, $\eta = 4.3 \times 10^6$ Pa s), and lithium disilicate (at $1.11T_g$, $\eta = 1.6 \times 10^8$ Pa s), there were clear signs of a *breakdown* of the SE/E equation at these viscosities. Nascimento and Zanotto demonstrated that viscosity data cannot be used to describe the transport part of the crystal growth (via the SE/E equation) in fragile glasses in the neighborhood of T_g.

In 2015, Schmelzer et al. (2015), derived at a relationship that allows a correlation of the decoupling temperature with the glass transition temperature and the liquid's fragility. The results were confirmed by experimental data. More recently, Cassar et al. (2017) suggested that above the temperature range $1.1T_g$–$1.3T_g$, crystal growth and viscous flow are controlled by the diffusion of silicon and lead in lead metasilicate glass. Below this temperature, crystal growth and viscous flow are more sluggish than the diffusion of silicon and lead. Therefore, T_d marks the temperature where *decoupling* between the (measured) cationic

diffusivity and the effective diffusivities calculated from viscosity and crystal growth rates occurs. These authors reasonably proposed that the nature or size of the diffusional entities controlling viscous flow and crystal growth below T_d is quite *different*; the slowest is the one controlling viscous flow, but *both* processes require cooperative movements of some larger structural units rather than jumps of only one or a few isolated atoms (Cassar et al. 2017).

Finally, Cassar et al. (2018a) tested and analyzed 4 different approaches to compute D_U. The classical approach ($D_U \sim \eta^{-1}$) and the fractional viscosity approach of Ediger ($D_U \sim \eta^{-\omega}$) were not able to describe the crystal growth rates near the glass transition temperature of supercooled diopside liquid ($CaMgSi_2O_6$). However, the proposed Arrhenian expression to calculate D_U—gradually changing from a viscosity-controlled to an Arrhenian-controlled process—was able to describe the available data in the whole temperature range and yielded the lowest uncertainty for the adjustable parameters. Their results corroborated the previous finding that viscous flow ceases to control the crystal growth process below the decoupling temperature. Figure 11 shows the overall results of this new approach, i.e., the regression of crystal growth rate data when D_U is calculated following the considerations that D_U gradually changes from viscosity-controlled to Arrhenian-controlled (see Eqn. 15). All available data are well described by the regression. The four adjustable parameters needed for this approach: σ, E_a, D_0, and T_d (see Eqn. 15). The regression yielded σ = 0.223(9) J/m^2, E_a = 650(50) kJ/mol, ln(D_0) = 31(6), and T_d = 1100(30) K, with RMS = 0.11 (D_0 in m^2/s) (Cassar et al. 2018a).

$$D_U = [x]\left[C\frac{T}{\eta_{eq}}\right] + [1-x]\left[D_0 \exp\left(-\frac{E_a}{RT}\right)\right] \quad (15)$$

where $x = \frac{1+\tanh(\alpha)}{2}$ (hyperbolic tangent function), $\alpha = \frac{T-T_d}{\phi T_d}$ ($\phi = 0.06$). Please note that $C = \frac{k_B}{d}$, k_B is the Boltzmann constant and d is the diameter of the moving entity that controls viscous flow, usually assumed to be equal to d_0 (jumping distance of a moving entity).

The above relationships, theory, and fundamentals allow one to describe the growth of crystals with smooth planar or spherical interfaces advancing in the liquid. However, more complex growth patterns do exist, and more complex models of growth are required to properly

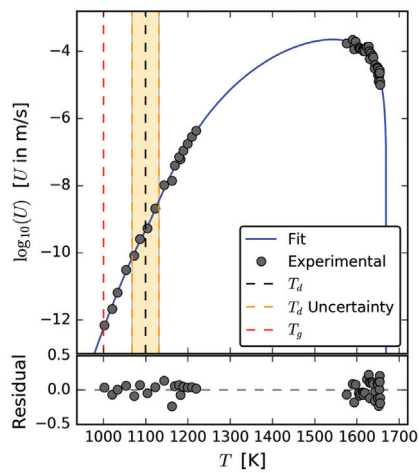

Figure 11. Regression curve of crystal growth rate data with D_U considering Arrhenian-controlled diffusion below T_d and Equation (15) (Cassar et al. 2018a). (T_d: decoupling temperature, T_g: glass transition temperature)

take into account possible interfacial instabilities, surface roughening, or other growth modes such as diffusion-limited aggregation (Jackson 2004). With such complex growth modes, a variety of intricate and beautiful crystal shapes may evolve, some of which are illustrated in Figure 12.

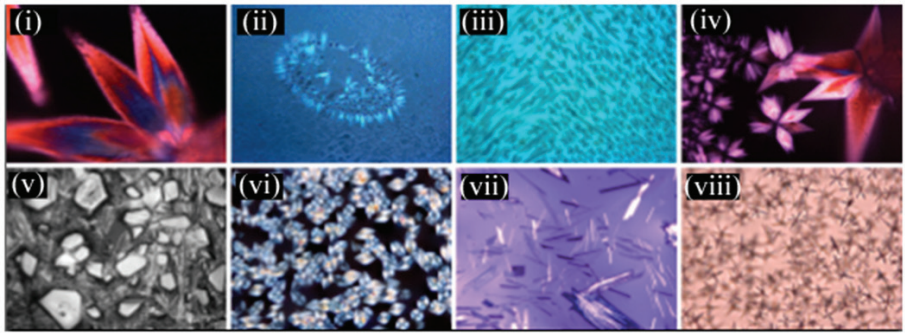

Figure 12. Crystal morphologies formed by nucleation and growth in oxide glass-formers as observed by optical microscopy (crystal sizes from 5 to 100 μm). From top left to bottom right: **(i, ii, iv)** LS crystals nucleated on defects of a $CaO{\cdot}Li_2O{\cdot}SiO_2$ glass surface during its preparation via melting–cooling **(iii)** Crystallization propagating from the surface towards the center of a $CaO{\cdot}Li_2O{\cdot}SiO_2$ glass specimen; lithium metasilicate crystals nucleated on two perpendicular surfaces and grew towards the sample center. **(v)** Surface of a $CaO{\cdot}Li_2O{\cdot}SiO_2$ glass sample after cooling a melt in a DSC furnace; the large-faceted and needle-like crystals are calcium and lithium metasilicates, respectively. **(vi)** Internal crystallization in a Ti-cordierite glass; pure stoichiometric cordierite ($2MgO{\cdot}2Al_2O{\cdot}5SiO_2$) glass underwent only surface nucleation, but the same glass doped with more than 6 mol% TiO_2 shows internal crystallization of μ-cordierite. **(vii)** Needle-like crystals in $CaO{\cdot}Li_2O{\cdot}SiO_2$ eutectic glass formed by internal crystallization in the temperature range between the *solidus* and the *liquidus;* these wollastonite crystals appear on the cooling path. **(viii)** Star-like NaF crystals inside a photo-thermo-refractive (PTR) glass (treatment at a high temperature near the solubility limit).

4. OVERALL CRYSTALLIZATION AND GLASS-FORMING ABILITY: THE JOHNSON–MEHL–AVRAMI–KOLMOGOROV APPROACH

Crystallization of supercooled liquids occurs by a combination of crystal nucleation and growth. The kinetics of such processes is usually described by a theory independently derived between 1937 and 1941 by Johnson, Mehl, Avrami, and Kolmogorov (Kolmogorov 1937; Johnson and Mehl 1939; Avrami 1939, 1940, 1941) denominated (JMAK theory). In this approach, the isothermal evolution of the total amount of the crystalline phase is described as a function of time, accounting simultaneously for nucleation and growth. The basic equations of this approach can be developed as follows.

Let us assume that, in a time interval $dt'(t', t'+dt')$, a number $dN(t') = J(t')[V - V_n(t')]$ of clusters of critical size is formed in the volume $[V - V_n(t')]$. Here, V is the initial volume of the glass-forming melt and $V_n(t')$ the volume already crystallized at time t'. These clusters grow and, at time t, occupy a volume

$$dV_n(t,t') = \omega_n J(t')\left(V - V_n(t')\right)dt'\left(\int_{t'}^{t} u(t'')dt''\right)^n \qquad (16)$$

where is a shape factor and the integral term describes the growth of the $dN(t')$ clusters formed at t' until time t, i.e., in the time interval $(t - t')$, the exponent n is the number of independent spatial directions of growth. Introducing the ratio, $\alpha_n(t)=(V_n(t)/V)$, between the current volume of the crystalline phase versus the initial volume of the glass-forming melt, one has

$$\alpha_n(t) = 1 - \exp\left(-\frac{\omega_n}{(n+1)} J u^n t^{(n+1)} \right) \tag{17}$$

Integration, i.e., taking the sum over all the time intervals dt' in the range of (0, t), yields

$$\alpha_n(t) = 1 - \exp\left(\omega_n \int_0^t J(t') dt' \left(\int_{t'}^t u(t'') dt'' \right)^n \right) \tag{18}$$

Provided the nucleation and growth rates are both constant; one reaches as a special case

$$\alpha_n(t) = 1 - \exp\left(-\frac{\omega_n}{(n+1)} J u^n t^{(n+1)} \right) \tag{19}$$

Conversely, if a number N_0 of supercritical clusters is formed immediately at time $t=0$, growing in n independent spatial directions, one arrives instead at

$$\alpha_n(t) = 1 - \exp\left(-g N_0 u^n t^n \right) \tag{20}$$

The analysis of the time dependence of the α_n-curves thus leads to the indirect determination of nucleation and growth kinetics.

The JMAK theory has been employed in numerous studies to analyze experimental data and determine the degree of crystallinity as a function of time in both isothermal and non-isothermal heat treatments of glasses. Emphasis has usually been given to the determination of the so-called Avrami coefficient $m = n+1$ obtained from the slopes of experimental $\ln[\ln(1-\alpha)^{-1}]$ *versus* $\ln(t)$ plots. An overview of various nucleation and growth mechanisms and the resulting values of the Avrami coefficient are given in Table 1 (Zheng et al. 2019). However, there is some uncertainty in such analyses, because different combinations of nucleation and growth laws may lead to the same Avrami coefficient. For this reason, a separate investigation of the growth kinetics may be required to reach definite conclusions (Johnson and Mehl 1939; Gutzow and Schmelzer 2013).

It is important to underline that the JMAK theory, as given by Equations (19) and (20), does not apply directly to non-isothermal processes. These two equations are derived on the assumption of constant nucleation and growth rates, which does not hold in non-isothermal processes. Therefore, in non-isothermal cases, the general relationships, Equations (17) and (18) must be employed to describe overall crystallization.

Such considerations must also be taken into account when the JMAK formalism is employed to determine whether a liquid will transform into a glass upon cooling or whether it will crystallize. Following Uhlmann (1982), one can consider a supercooled frozen-in liquid a glass if, after vitrification, the volume fraction of the crystal phase does not exceed a certain value of, say, 10^{-6} (the detection limit by microscopy). Using appropriate expressions for nucleation and growth rates, one can then compute (through Eqn. 19 for isothermal conditions) the time required to reach the volume fractions thus defined. In this way, one arrives at the so-called *T*(ime)*T*(emperature)*T*(ransformation)-curves (*TTT*-curves) exemplified in Figure 13 (cf. also Kelton and Greer 2010 and Fig. 10.8 in Gutzow and Schmelzer 2013). These curves give some insight into the characteristic time scales required to prevent measurable crystallization effects. One should keep in mind, however, that these curves overestimate the critical cooling rates for glass formation by about one order of magnitude because, as mentioned earlier, crystallization upon cooling proceeds under non-isothermal conditions.

Table 1. Values of the Avrami exponent (n) for several crystallization mechanisms (Zheng et al. 2019).

Polymorphic change, interface-controlled growth	***n***	**Diffusion-controlled growth**	*n*
Increasing nucleation rate, 3D	> 4	Increasing nucleation rate, 3D	> 2.5
Constant nucleation rate, 3D	4	Constant nucleation rate, 3D	2.5
Decreasing nucleation rate, 3D	3–4	Decreasing nucleation rate, 3D	1.5–2.5
Zero nucleation rate (nucleation site saturation) 3D	3	Constant nucleation rate, 2D	2
Constant nucleation rate, 2-D (plates)	3	Zero nucleation rate, 3D	1.5
Zero nucleation rate, 2-D (plates)	2	Constant nucleation rate, 1D	1.5
Constant nucleation rate (nucleation site saturation), 1D	2	Zero nucleation rate, 2D	1
Zero nucleation rate, 1D (needles)	1	Zero nucleation rate, 1D	0.5

Note: D: growth dimensionality

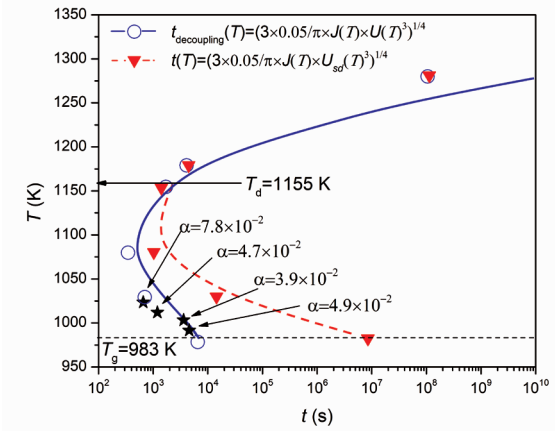

Figure 13. Simulated *TTT*-curves for a $BaO{\cdot}2TiO_2{\cdot}2SiO_2$ glass with crystallized volume fraction α = 0.05 using, in one approach, the screw dislocation growth model both above and below T_d (screw dislocation–**dashed line, triangles**), and in the other the Arrhenius equation below T_d (**solid line, spheres**). Experimental data points (**black stars**) obtained at 993, 1003, 1013, and 1023 K. (T_d: decoupling temperature). [Reprinted from Rodrigues and Zanotto (2012) Evaluation of the guided random parametrization method for critical cooling rate calculations. J Non-Cryst Solids 358:2626–34 Copyright (2012), with permission from Elsevier.]

Using experimental crystal nucleation and growth rate data, Rodrigues and Zanotto (2012) calculated *TTT*-curves for different isothermal and non-isothermal crystallization situations. They also accounted for the breakdown of the Stokes–Einstein–Eyring (SEE) equation at a temperature T_b (somewhat higher than T_g) where the effective diffusion coefficient that controls crystal growth decouples from the value of diffusivity calculated by the SEE equation (Eqn. 7). In Figure 13, we show an example of such a curve for a stoichiometric $BaO{\cdot}2TiO_2{\cdot}2SiO_2$ glass, which undergoes copious internal homogenous crystal nucleation. The agreement with experimental data (which, in this case, were also obtained in isothermal conditions) is quite impressive, indicating that the JMAK equation is accurate if all the assumptions involved in its

derivation are met. From such curves, one can calculate very important properties of supercooled liquids—namely the glass-forming ability, and the glass stability against crystallization on heating.

Glass forming ability (GFA) is the propensity of a melt to vitrify upon cooling. Quantifying glass-forming ability is of utmost importance for the design of new glass compositions, but it is a laborious, time-consuming process. Several methods are available to estimate the GFA (Shelby 2005). The ease of glass formation can be defined by the critical cooling rate (CCR) required to prevent crystallization of a certain sample. The critical cooling rate is a quantitative measure of the ability of a liquid to vitrify and is defined as the slowest rate at which a melt can be cooled from its liquidus temperature (T_m) to below the glass transition temperature (T_g)—which is composition and thermal history dependent—without "detectable" crystallization, i.e., a crystallized volume fraction normally assumed to be in the range of 10^{-6}–10^{-2} (such as α in Fig. 13). The smaller the CCR, the greater the glass forming ability of a liquid. Thus, CCR is a very important characteristic parameter of liquids that should be known to predict the ease or difficulty of glass formation, and, hence, to determine the processing conditions of any glass (Scherer 1991). For instance, the CCR of metallic glasses lie in between 10^6 to 10^1 K/s, whereas commercial oxide glasses, such as window glass, have a CCR of $< 10^{-2}$ K/s.

Figure 14 shows the TTT-curves of two glass-forming melts whose internal (homogeneous) nucleation rates differ by 15 orders of magnitude. Anorthite glass shows a maximum nucleation rate of approximately 10^2 $m^{-3}.s^{-1}$, whereas fresnoite has a maximum of 10^{17} $m^{-3}.s^{-1}$. Even for a small density of surface nucleation sites (N_s), the nose of the TTT curves for heterogeneous surface nucleation leads to shorter times compared to the nose of the homogeneous nucleation TTT curves. The equivalent N_S for a heterogeneous TTT curve to exhibit the same CCR as the homogeneous case would be around 10^{-2} and 10^{-1} sites/m^2 for anorthite and fresnoite glasses, respectively.

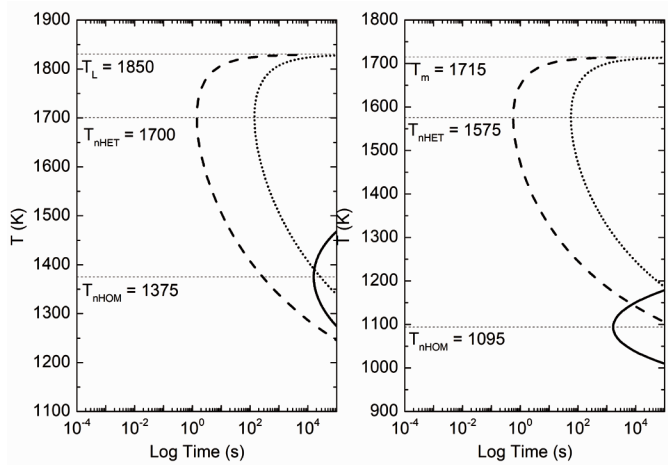

Figure 14. Temperature *versus* time in log scale: TTT curves for anorthite ($CaO.Al_2O_3.2SiO_2$) (**left**), and fresnoite ($2BaO.TiO_2.2SiO_2$) (**right**) considering homogeneous nucleation (—) and heterogeneous surface nucleation for $N_S = 10^5$ (– – –) and $N_S = 10^1$ (·····). The nose times seem to be close to each other, however the time scale is logarithmic. (Jiusti et al. 2020)

Above all, even more important than measuring or estimating the GFA of different substances is the ability to predict the GFA as a function of composition. While this is not yet possible for complex, multicomponent systems, research efforts should and are moving into this direction (Varshneya and Mauro 2019; Zheng et al. 2019). For example, Jiusti et al. (2020) have recently

derived a mother parameter, GFA = 1/CCR $\propto [U(T_{max}) \times T_L]^{-1}$, which strongly correlates with the experimental critical cooling rates of oxide glass-formers. A simplified version derived from the mother parameter—which does not need (scarce) crystal growth rate data and only relies on (easily measurable or calculable) viscosity, η, and T_L—GFA $\propto [\eta(T_L)/T_L^2]$—also correlates well with the CCR of several oxide compositions. This new GFA parameter corroborates the widespread concept that substances having high viscosity at T_L, and a low T_L can be easily vitrified, and provides a powerful tool for the quest and design of novel glasses.

4.1 Glass stability against crystallization

While GFA is defined as the resistance to crystallization of a supercooled liquid during cooling, *glass stability* is defined as the resistance to devitrification of a glass or supercoooled liquid during heating. Glass forming ability is most important during processes requiring vitrification, while glass stability (GS) is very important during operations involving thermal treatment of an existing glass, such as annealing, tempering or treatment for ceramization. Although these two properties are not identical, they are frequently confused in the literature and technological practice. It is often (reasonably) assumed that poor glass-forming ability automatically leads to poor glass stability, and vice-versa (Shelby 2005). GS is frequently characterized by the difference between the onset of the glass transformation region (T_g) and the DSC crystallization peak (T_c) or onset of crystallization peak (T_x) for a sample heated at a particular rate. A drawback of this method is that these two temperatures depend not only on the chemical composition but also on glass particle size and heating rate; hence these two experimental parameters should be kept constant for a proper evaluation of glass stability. Some authors argued that the quantity ($T_c - T_g$) should be normalized by T_g, T_c, T_x, or T_m of the crystalline phase, to compare the behavior of glasses which crystallize in very different temperature ranges. The most well-known parameter is the Hrubý number, which is defined by $H_b = (T_x - T_g)/(T_c - T_g)$. Stable glasses have a $H_b > 0.4$.

However, there is no unanimously accepted criterion for glass stability. As long as samples of different compositions are compared using identical characteristics (particle size and heating rate), several of the proposed parameters (e.g., Hrubý), especially those containing all the three characteristic temperatures, yield similar results. Interested readers are encouraged to refer to a comprehensive review by Zheng et al. (2019), which compares various GS parameters determined by DSC.

5. PERSPECTIVES

Significant advances in the understanding and control of crystal nucleation and growth processes in glass-forming liquids have been achieved over the last five decades. It is now well-established that all materials can vitrify when subjected to sufficiently fast cooling from the liquid state. Thus, novel reluctant glass-forming materials, such as certain metallic and chalcogenide glasses, with unusual properties, have been successfully obtained by very fast quenching. Moreover, controlled, catalyzed internal crystallization of specific glasses has led to a variety of advanced glass-ceramics that are now available on the market. More profound insights into glass crystallization processes, such as precise prediction of nucleation and growth rates, and critical cooling rates for glass formation, based solely on materials properties, will depend critically on new developments in nucleation and growth theories and computer simulations. Artificial Intelligence techniques could be a major player in this context (Cassar et al. 2018b, 2021; Alcobaça et al. 2020; Montazerian et al. 2020).

Furthermore, in their recent comprehensive review, Zheng et al. (2019) elaborated on the versatility and utility of several differential scanning calorimetry (DSC) techniques for examining the dynamics related to nucleation, growth, glass-forming ability and stability.

For example, DSC is very useful for providing estimates of the temperature range where significant nucleation occurs. When properly used, isothermal DSC runs can yield useful information regarding crystallization processes, including the crystal number density, nucleation and growth kinetics, the activation energy for overall crystallization, and the Avrami constant. In addition to DSC, advanced instruments, such as Transmission Electron Microscopy (TEM), Anomalous Small Angle X-ray Scattering (ASAXS), Small-angle Neutron Scattering (SANS), X-ray Absorption Spectroscopy (XAS), Raman Spectroscopy (RS), Nuclear Magnetic Resonance (NMR), Advanced Optical Spectroscopy (OS) and others have been recently employed to study nuclei of critical sizes and medium range order in glasses. They provide critical insight into the complicated and rapidly changing environments in which crystallization happens, helping us to shed light over nucleation and crystallization processes in glass-forming materials. Interested readers are referred to a recent book authored by Neuville and coworkers (Neuville et al. 2017).

Despite the many advances achieved in understanding crystallization, some key problems remain open. Among the most notable, we remark the following:

(i) Specification of the bulk (structure, composition, density) and surface properties of the critical nuclei as a function of size.

(ii) Description of the temperature dependence of the crystal nucleus–liquid interfacial energy.

(iii) The applicability of the Stokes–Einstein–Eyring (viscosity) relationship in calculating the effective diffusion coefficients that control crystal nucleation.

(iv) Unveiling the cause of the reported breakdown of the CNT in describing the temperature dependence of experimental nucleation rates below T_g.

(v) A deeper understanding of the relationship between the molecular structure of glass-forming melts and the nucleation mechanism.

(vi) The relation between the sizes of supercritical nuclei vis-à-vis the sizes of co-operatively rearranging regions (CRR) of heterogeneous dynamics (DHD) existing in the structure of viscous liquids

(vii) Comparison of the estimated (by extrapolation) structural relaxation time and the characteristic time for crystallization of glass-forming liquids at the (predicted) Kauzmann temperature, T_K. Such a comparison could resolve the paradox, following Kauzmann's suggestion of the possibility that the putative state of negative entropy may never be reached because at such temperatures, crystallization would always intervene before structural relaxation of any SCL.

All these problems, in addition to several others not mentioned here, such as the development of novel glasses and glass-ceramics, having exotic, unusual compositions and combination of properties, corroborate that glass crystallization is a very dynamic, exciting research topic.

ACKNOWLEDGMENTS

EDZ is indebted to his numerous co-workers and students for the enjoyable and educative joint research on glass crystallization over the past 45 years. Generous and continuous funding by the Brazilian agencies CAPES, CNPq, and São Paulo Research Foundation, FAPESP (CEPID grant #2013/07793-6 and #2015/13314-9) is much appreciated.

REFERENCES

Abyzov AS, Fokin VM, Rodrigues AM, Zanotto ED, Schmelzer JWP (2016) The effect of elastic stresses on the thermodynamic barrier for crystal nucleation. J Non-Cryst Solids 432:325–333

Abyzov AS, Fokin VM, Zanotto ED (2018) Predicting homogeneous nucleation rates in silicate glass-formers. J Non-Cryst Solids 500:231–234

Alcobaça E, Mastelini SM, Botari T, Pimentel BA, Cassar DR, de Carvalho ACPDLF, Zanotto ED (2020) Explainable machine learning algorithms for predicting glass transition temperatures. Acta Mater 188:92–100

Avrami M (1939) Kinetics of phase change. I General theory. J Chem Phys 7:1103–12

Avrami M (1940) Kinetics of phase change. II Transformation time relations for random distribution of nuclei. J Chem Phys 8:212–24

Avrami M (1941) Kinetics of phase change. III Granulation, phase change, and microstructure kinetics of phase change. J Chem Phys 9:177–84

Berthier L (2011) Trend: dynamic heterogeneity in amorphous materials. Physics 4:42

Cassar DR, Lancelotti RF, Nuernberg R, Nascimento MLF, Rodrigues AM, Diz LT, Zanotto ED (2017) Elemental and cooperative diffusion in a liquid, supercooled liquid and glass resolved. J Chem Phys 147:014501

Cassar DR, Rodrigues AM, Nascimento MLF, Zanotto ED (2018a) The diffusion coefficient controlling crystal growth in a silicate glass-former. Inter J Appl Glass Sci 9:373–382

Cassar DR, de Carvalho ACPLF, Zanotto ED (2018b) Predicting glass transition temperatures using neural networks. Acta Mater 159:249–256

Cassar DR, Serra AH, Peitl O, Zanotto ED (2020) Critical assessment of the alleged failure of the Classical Nucleation Theory at low temperatures. J Non-Cryst Solids 547:120297

Cassar DR, Santos GG, Zanotto ED (2021) Designing optical glasses by machine learning coupled with a genetic algorithm. Ceram Inter 47: 10555–10564

Deubener J, Brückner R, Sternitzke M (1993) Induction time analysis of nucleation and crystal growth in di- and metasilicate glasses. J Non-Cryst Solids 163:1–12

Ediger MD (2000) Spatially heterogeneous dynamics in supercooled liquids. Ann Rev Phys Chem 51:99–128

Ediger MD (2008) Crystal growth kinetics exhibit a fragility-dependent decoupling from viscosity. J Chem Phys 128:034709

Flenner E, Szamel G (2010) Dynamic heterogeneity in a glass forming fluid: Susceptibility, structure factor, and correlation length. Phys Rev Lett 105:217801

Fokin VM, Potapov OV, Zanotto ED, Spiandorello FM, Ugolkov VL, Pevzner BZ (2003) Mutant crystals in $Na_2O{\cdot}2CaO{\cdot}3SiO_2$ glasses. J Non-Cryst Solids 331:240–253

Fokin VM, Zanotto ED, Yuritsyn NS, Schmelzer JWP (2006) Homogeneous crystal nucleation in silicate glasses: A 40 years perspective. J Non-Cryst Solids 352:2681–2714

Fokin VM, Schmelzer JWP, Nascimento MLF, Zanotto ED (2007) Diffusion coefficients for crystal nucleation and growth in deeply undercooled glass-forming liquids. J Chem Phys 126:234507

Fokin VM, Abyzov AS, Zanotto ED, Cassar DR, Rodrigues AM, Schmelzer JWP (2016) Crystal nucleation in glass-forming liquids: Variation of the size of the "structural units" with temperature. J Non-Cryst Solids 447:35–44

Fokin VM, Abyzov AS, Rodrigues AM, Pompermayer RZ, Macena GS, Zanotto ED, Ferreira EB (2019) Effect of non-stoichiometry on the crystal nucleation and growth in oxide glasses. Acta Mater 180:317–328

Gibbs JW (1926) Collected Works, vol. 1, Thermodynamics. Longman, New York

Gupta PK, Cassar DR, Zanotto ED (2016) Role of dynamic heterogeneities in crystal nucleation kinetics in an oxide supercooled liquid. J Chem Phys 145:211920

Gutzow IS, Schmelzer JWP (2013) The Vitreous State: Thermodynamics, Structure, Rheology, and Crystallization. Springer, 2nd enlarged ed. Heidelberg

Henritzi P, Bormuth A, Klameth F, Vogel M (2015) A molecular dynamics simulations study on the relations between dynamical heterogeneity, structural relaxation, and self-diffusion in viscous liquids. J Chem Phys 143:164502

Höland W, Beall GH (2013) Glass-Ceramic Technology. Wiley, Hoboken, New Jersey

Jackson KA (2004) Kinetic Processes. Wiley-VCH, Weinheim

Jiusti J, Zanotto ED, Cassar DR, Andreeta MRB (2020) Viscosity and liquidus based predictor of glass-forming ability of oxide glasses. J Am Ceram Soc 103:921–932

Johari GP, Schmelzer JWP (2014) Crystal nucleation and growth in glass-forming systems: Some new results and open problems. *In:* Glass: Selected Properties and Crystallization. Schmelzer JWP (ed) de Gruyter, Berlin p 531–590

Johnson WA, Mehl R (1939) Reaction kinetics in processes of nucleation and growth. Trans AIME 135:416–58

Kashchiev D (2000) Nucleation : Basic Theory with Applications. Butterworth Heinemann, Oxford

Kauzmann W (1948) The nature of the glassy state and the behavior of liquids at low temperatures. Chem Rev 43:219–256

Kelton KF, Greer AL (2010) Nucleation in Condensed Matter: Applications in Materials and Biology. Elsevier, Amsterdam

Kolmogorov AN (1937) On the statistical theory of crystallization of metals. Izv Akad Nauk SSSR 3:355–59

Macena GS, Abyzov AS, Fokin VM, Zanotto ED, Ferreira EB (2020) Off-stoichiometry effects on crystal nucleation and growth kinetics in soda-lime-silicate glasses. The combeite (Na_2O•2CaO•3SiO_2)—devitrite (Na_2O•3CaO•6SiO_2) joint. Ac ta Mater 196:191–199
Montazerian M, Singh SP, Zanotto ED (2015) An analysis of glass-ceramic research and commercialization. Am Ceram Soc Bull 94:30–35
Montazerian M, Zanotto ED, Mauro JC (2020) Model-driven design of bioactive glasses: from molecular dynamics through machine learning. Inter Mater Rev 65(5): 297–321
Morey GW (1954) The Properties of Glass. Reinhold Publishers, New York
Nascimento MLF, Zanotto ED (2006) Mechanisms and dynamics of crystal growth, viscous flow, and self-diffusion in silica glass. Phys Rev B—Condens Matter and Mater Phys 73:024209
Nascimento MLF, Zanotto ED (2010) Does viscosity describe the kinetic barrier for crystal growth from the liquidus to the glass transition? J Chem Phys 133:174701
Nascimento MLF, Fokin VM, Zanotto ED, Abyzov AS (2011) Dynamic processes in a silicate liquid from above to below the glass transition. J Chem Phys 135:194703
Neuville D, Cornier L, Caurant D, Montagne L (eds) (2017) From Glass to Crystal: Nucleation, Growth and Phase Separation, from Research to Applications. EDP Science, London
Prado SCC, Rino JP, Zanotto ED (2019) Successful test of the classical nucleation theory by molecular dynamic simulations of BaS. Comp Mater Sci 161:99–106
Reis RMCV, Fokin VM, Zanotto ED, Lucas P (2016) Determination of crystal growth rates in glasses over a temperature range using a single DSC run. J Am Ceram Soc 99:2001–2008
Rodrigues BP, Zanotto ED (2012) Evaluation of the guided random parametrization method for critical cooling rate calculations. J Non-Cryst Solids 358:2626–34
Scherer GW (1991) Chapter 3: Glass and amorphous materials. *In:* Materials Science and Technology. Vol 9. Cahn RW, Haasen P, Kramer EJ (eds), VCH Publications, New York
Schmelzer JWP, Schick C (2012) Dependence of crystallization processes of glass-forming melts on melt history: A theoretical approach to a quantitative treatment. Phys Chem Glass Eur J Glas Sci Technol Part B 53:99–106
Schmelzer JWP, Abyzov AS, Fokin VM, Schick C, Zanotto ED (2015) Crystallization in glass-forming liquids: Effects of decoupling of diffusion and viscosity on crystal growth. J Non-Cryst Solids 429:45–53
Separdar L, Rino JP, Zanotto ED (2021) Molecular dynamics simulations of spontaneous and seeded nucleation and theoretical calculations for zinc selenide. Comp Mater Sci 187:110124
Shelby JE (2005) Introduction to Glass Science and Technology. The Royal Society of Chemistry, Lonton
Slezov VV (1999) Kinetics of First-Order Phase Transitions. Wiley-VCH, Weinheim
Tammann G (1898) Über die Abhängigkeit der Zahl der Kerne. Z Phys Chem 25:441–479
Tipeev AO, Zanotto ED, Rino JP (2018) Diffusivity, interfacial free energy, and crystal nucleation in a supercooled Lennard–Jones liquid. J Phys Chem C 122:28884–28894
Tipeev AO, Zanotto ED, Rino JP (2020) Crystal nucleation kinetics in supercooled germanium: MD simulations versus experimental data. J Phys Chem B 124:7979–7988
Uhlmann DR (1982) Crystal growth in glass-forming liquids: A ten-year perspective. *In:* Advances in Ceramics. Vol 4. Simmons JH, Uhlmann DR, Beall GH (eds), American Ceramic Society, Columbus, p 80–124
Varshneya AK, Mauro JC (2019) Fundamentals of Inorganic Glasses. 3rd ed. Elsevier, Amsterdam
Volmer M (1939) Kinetik der Phasenbildung. Th. Steinkopff, Dresden
Zanotto ED (2010) A bright future for glass-ceramics. Am Ceram Soc Bull 89:19–27
Zanotto ED (2013) Crystals in Glass: A Hidden Beauty. Wiley, Hoboken New Jersey
Zanotto ED, Cassar DR (2018) The race within supercooled liquids—Relaxation versus crystallization. J Chem Phys 149:02450
Zanotto ED, Mauro JC (2017) The glassy state of matter: Its definition and ultimate fate. J Non-Cryst Solids 471:490–495
Zanotto ED, Tsuchida JE, Schneider JF, Eckert H (2015) Thirty-year quest for structure-nucleation relationships in oxide glasses. Inter Mater Rev 60:376–391
Zheng Q, Zhang Y, Montazerian M, Gulbiten O, Mauro JC, Zanotto ED, Yue Y (2019) Understanding glass through differential scanning calorimetry. Chem Rev 119:7848–7939